A PARTICLE SWARM OPTIMIZATION APPROACH FOR CONTROLLER DESIGN IN WECS EQUIPPED WITH DFIG

ASSISTANT PROFESSOR: ***Dr. Y. SUMANTH***

M. VENKATESH[1], K. VENKATA SAI[2], K. VAMSI CHAITANYA[3], N.S.S. PRAKASH[4]

[1]STUDENT, [2]STUDENT, [3]STUDENT, [4]STUDENT

DEPARTMENT OF ELECTRICAL & ELECTRONICS ENGINEERING,

R.V.R & J.C. COLLEGE OF ENGINEERING, GUNTUR, ANDHRA PRADESH, INDIA.

ABSTRACT

This paper focuses on the design of optimal PI controller parameters for a Wind Energy Conversion System (WECS) equipped with a Doubly Fed Induction Generator (DFIG). The study is conducted on a MW-scale WECS connected to a distribution network. The variable speed DFIG is typically controlled by a set of PI controllers. However, due to the nonlinearity and complexity of the system, determining the optimal controller parameters can be challenging. In this paper, Particle Swarm Optimization (PSO) is employed to tune the parameters of the rotor-side converter controller of the DFIG. To enhance performance and restrict controller action, an optimization problem is formulated by selecting appropriate objective functions and constraints. The system's performance is evaluated under various conditions, including grid voltage sag due to remote faults, single-phase-to-ground faults, and wind speed changes. A comparison is made between the performance with PI controller parameters and PSO-optimized controller parameters. Simulation results demonstrate the improved transient behaviour of the WECS equipped with DFIG under the specified test conditions. Simulation results were verified through SIMULINK.

I. INTRODUCTION:

Energy consumption is rapidly increasing worldwide as we strive to improve our living standards. However, our fossil fuel and nuclear resources are limited. This has led to a growing need to find renewable or virtually inexhaustible energy sources. The world is increasingly turning to environmentally clean and safe renewable energy sources to sustain life's natural foundations: soil, water, air, and achieve CO2 neutrality. Wind power has emerged as a primary renewable energy source in many countries. Variable speed wind turbines equipped with doubly fed induction generators (DFIGs) are commonly used in large wind farms due to their broad operating range, from sub-synchronous to super-synchronous speeds. DFIGs are popular because they can provide power at constant voltage and frequency even as the rotor speed varies. This concept also allows for overall system power factor control. DFIGs offer additional benefits, including reduced mechanical stresses on wind turbines, noise reduction, fewer requirements for pitch angle controllers, lower rating converters, and thus improved overall efficiency.

As a result, wind energy conversion systems (WECS) may soon begin to impact the behavior of electrical power systems. Therefore, a reliable model of WECS is essential to study its effects on power system behavior. The concept of WECS involves DFIGs that track optimal power at a reference terminal voltage. Various controllers are integrated into the system, including power, reactive power/voltage, current, and pitch angle controllers. A range of control design schemes for variable speed WECS has been utilized, often relying on PI controllers for their proven reliability and robust performance. The design of these controllers is typically described using conventional methods. In this system, the inner loop controllers operate much faster than the outer loop controllers, with all methods demonstrating satisfactory results. With an increasing number of WECS being connected to the network, new network codes have been issued. These codes require wind generators to support the network within a specified

power factor range and to continue operating without disconnection even during a defined voltage drop. Consequently, it is crucial to accurately estimate the controller parameters to optimize system performance.

The performance of the system largely depends on the actions of the rotor-side converter controller. Therefore, this study focuses on optimizing the parameters of the rotor-side converter PI current controller to achieve the desired optimal performance of the WECS. It is assumed that the grid-side converter controllers effectively control the link voltage at the reference level. The study utilizes particle swarm optimization (PSO) as a searching algorithm, implementing objective functions to optimize the parameters of the rotor-side converter current controller. Swarm intelligence, with its use of mobile agents, offers several advantages such as scalability, fault tolerance, adaptation, speed, modularity, autonomy, and parallelism. The optimization problem is formulated with two objective functions to tune the parameters of the rotor-side converter current controller, aiming for improved system response. These objective functions are based on various performance metrics including peak overshoot ratio, rise time, peak time, settling time, set point crossing time, and steady-state error. Simulation results demonstrate the system's responses under different test conditions such as voltage sag at the grid, single-phase-to-ground faults, and changes in wind speed. The performance of the overall system is evaluated using both the Pl controller and the PSO-optimized PI controller.

II. RELATED WORK:

2.1 Wind Energy Conversion System

The energy present in moving air cannot be completely converted into another form of energy with 100% efficiency by any energy converter, such as a wind turbine in the case of a Wind Energy Conversion System (WECS) [10]. However, a variable-speed WECS can store the varying incoming wind power as rotational energy by adjusting the speed of the wind turbine. This approach allows for increased energy production with reduced stress on the mechanical structure. The basic configuration of a grid-connected WECS equipped with a Doubly Fed Induction Generator (DFIG) is illustrated in Figure 1. The key components of the wind turbine include rotor blades and a shaft that extract energy from the wind. The turbine unit then converts this energy into mechanical power, which is further converted into electrical power by a generator. The modeling of the various subsystems is explained below.

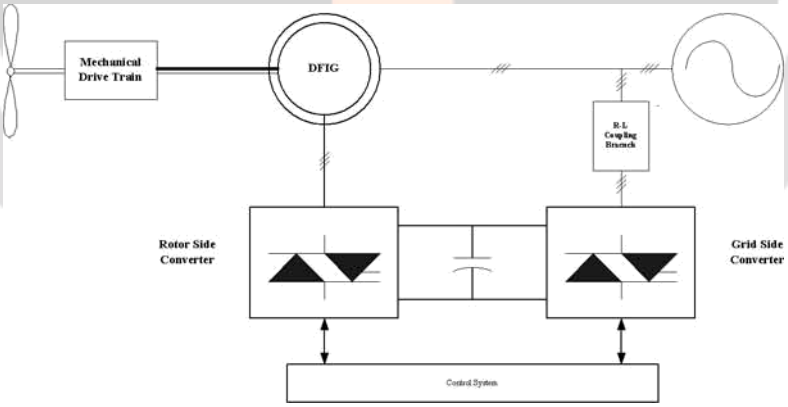

Fig. 1: The basic configuration of a WECS equipped with DFIG

2.2 Wind Turbine

A simplified aerodynamics model is employed, utilizing the average wind speed as an input. As the air flows through an area A, which corresponds to the area swept by the rotor blades, with a velocity v, the power carried by the air (taking into account air density) can be calculated as [10]: $P_{wind} = \frac{1}{2}\rho A v3$

The mechanical power P mech captured by a wind turbine depends on its performance coefficient Cp and can be represented by equation (1.11). $P_{mech} = \frac{1}{2} C\text{p}\ (\lambda, \theta)\rho\pi\Re 2v3$ (1)

The performance coefficient Cp can be defined as the fraction of mechanical power produced from the total power available from the wind, and it is specific to each turbine [4, 11-12].

$$Cp\,(\lambda,\theta) = c1*\{\frac{c2}{\lambda_i} - c3*\theta - c4\}\; e^{-c5/\lambda i} + c6 * \lambda I \quad (2)$$

with: $\frac{1}{\lambda_i} = \frac{1}{\lambda+0.08\theta} - \frac{0.035}{\theta^3+1}$ and $\lambda = \frac{\varpi \Re}{v}$

2.3 DFIG Model

To accommodate a broad operating range, ranging from sub-synchronous to super-synchronous speeds, a back-to-back converter is linked to the rotor. This setup allows the Doubly Fed Induction Generator (DFIG) to transmit power to the grid through both the stator and the rotor. Additionally, depending on the rotor's rotational speed, the rotor can also absorb power.

The voltage equations that describe the balanced steady-state operation of an induction machine can be derived in various manners. These equations, in complex form, for an induction machine can be expressed as follows [11, 13]:

$$v_s = Z_s i_s + Z_m i_r \quad (3)$$
$$v_r = Z_d i_s + Z_r i_r$$

In equation (3), the complex operational impedance expressions include a derivative operator p.

The impedances Z can be defined as: $\boldsymbol{Z_s} = R_s + (L_s + L_m)(p + j\omega_s)$

$$\boldsymbol{Z_m} = L_m(p + j\omega_s)$$
$$\boldsymbol{Z_d} = L_m(p + j(\omega_s - \omega_r)) \quad (4)$$
$$\boldsymbol{Z_r} = R_r + (L_r + L_m)(p + j(\omega_s - \omega_r))$$

The operating principle of a Doubly Fed Induction Generator (DFIG) can be examined using the widely used d-q model. Under balanced steady-state conditions, the d and q variables exhibit sinusoidal behavior in all reference frames, except in the synchronously rotating reference frame, where they remain constant. In this context, the reference frame is moving at synchronous speed [5, 14-17].

The d-q components of voltages are described as under: $v_{ds} = R_s\, i_{ds} + \frac{d\psi_{ds}}{dt} - \omega_s \psi_{qs}$

$$v_{qs} = R_s\, i_{qs} + \frac{d\psi_{qs}}{dt} - \omega_s \psi_{ds}$$
$$v_{dr} = R_r\, i_{dr} + \frac{d\psi_{dr}}{dt} - (\omega_s - \omega_r)\psi_{qr} \quad (5)$$
$$v_{qr} = R_r\, i_{qr} + \frac{d\psi_{qr}}{dt} - (\omega_s - \omega_r)\psi_{dr}$$

where ψ stands for flux linkage and express as: $\psi_{ds} = L_{ss} i_{ds} + L_m i_{dr}$

$$\psi_{qs} = L_{ss} i_{qs} + L_m i_{qr}$$
$$\psi_{dr} = L_{rr} i_{dr} + L_m i_{ds} \quad (6)$$
$$\psi_{qr} = L_{rr} i_{qr} + L_m i_{qs}$$

And also: $L_{ss} = L_s + L_m$

$$L_{rr} = L_r + L_m \quad (7)$$

The dynamic equations of an induction machine in the dq reference frame, which is rotating at synchronous speed, are described above.

2.4 Mechanical System

For a basic mechanical system with inertia H and damping F, the rotor swing equation is given by equation (4):

$$T_e = 2H\omega_r + F\omega_r + T_m \quad (8)$$

The electromagnetic torque with the positive sequence component is expressed as:

$$T_e = L_m(i_{qs}i_{dr} - i_{ds}i_{qr}) = (i_{qs}\omega_{ds} - i_{ds}\omega_{qs}) \quad (9)$$

2.5 Back-To-Back Converter

The frequency converter that powers the rotor of a Doubly Fed Induction Generator (DFIG) comprises two voltage source inverters connected back-to-back. It is linked between the DFIG rotor and the grid, as illustrated in Fig 1.

Here, we present the dynamics of the DC-link capacitor, and we add the differential equation of the DC-link capacitor to the DFIG model. The stored energy W_{dc} in the DC-link capacitor, with capacitance C and voltage v_{dc} can be considered as [18]: $W_{dc} = \int P_{dc}d\tau = \frac{1}{2}Cv_{dc}^2$ (10)

This model computes the changes in the DC-link capacitor voltage v_{dc} based on the power to the DC-link. The value of the DC-link voltage v_{dc} is determined by the input power P_{dc} as follows:

$$P_{dc} = P_g - P_r = [Re(v_s i_g) - Re(v_r i_r)] \quad (11)$$

and $$\frac{dv_{dc}}{dt} = \frac{1}{Cv_{dc}}[Re(v_s i_g) - Re(v_r i_r)] \quad (12)$$

The dynamics of the DC-link capacitor, with i_{og} and i_{or} being the grid-side and rotor-side converter DC-link currents respectively, as illustrated in Figure 2, can be described as follows [5]:

$$C\frac{dv_{dc}}{dt} = [i_{og} - i_{or}] \quad (13)$$

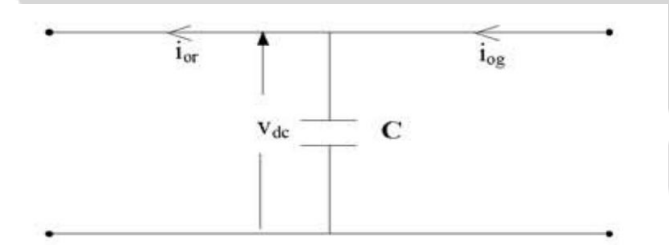

Fig.2: Intermediate dc-link circuit model

For the initialization process, it is assumed that the charging current and discharging current are equal, and the power losses in the converter mains are neglected: $i_{og} = i_{or}$ and $P_g = P_r$ (14)

III. Control Strategy:

The performance of a Wind Energy Conversion System (WECS) equipped with a Doubly Fed Induction Generator (DFIG) is assessed based on its ability to capture maximum power from the wind at a reference voltage. Achieving the desired performance requires accurate estimation of converter current controller parameters. The objective of the grid-side converter control is to supply the DC-link with the necessary voltage to maintain the DC-link voltage v_{dc} at a preset reference value, V_{dc_ref}, regardless of the magnitude and direction of the rotor power. The rotor-side converter is connected to the same DC-link. This converter injects the appropriate rotor voltage to ensure that

the DFIG tracks the maximum power curve and maintains the voltage at a reference level [|12, 18-19|]. The converters are treated as lossless devices, and the switches are assumed to be ideal.

3.1. Field Orientation:

The principles and outcomes of the vector control scheme employed in Doubly Fed Induction Generators (DFIGs) are rooted in the classical concept of field orientation. Consequently, selecting a suitable coordinate system is crucial for designing the control structure. Transforming control variables and machine variables from one coordinate system to another is essential. Several options for choosing the field orientation include stator-flux orientation, stator-voltage orientation, and air-gap-flux orientation [5, 16].

In this context, the Doubly Fed Induction Generator (DFIG) is controlled in a synchronous frame, with the d-axis aligned along the stator flux linkage [20]. $\psi_{ds} = \psi_s \quad and \quad \psi_{qs} = 0;$ (15)

The d-q coordinate stator voltage, with ψ_s being constant and neglecting stator resistance, can be expressed as:

$$v_{ds} = 0 \quad and \quad v_{qs} = V_s = \omega_s \psi_{ds} \tag{16}$$

As a result, the stator active power P_s and reactive power Q_s are:

$$P_s = v_{qs} i_{qs} = -V_s \left(\frac{L_m}{L_{ss}}\right) i_{qr} = -\omega_s \psi_{ds} \left(\frac{L_m}{L_{ss}}\right) i_{qr} \tag{17}$$

$$Q_s = v_{qs} i_{ds} = \omega_s \psi_{ds} \left(\frac{1}{L_{ss}}\right) (\psi_{ds} - L_m i_{qr}) \tag{18}$$

In this manner, a decoupled control for active power and reactive power, or voltage control, is achieved. This enables the regulation of two rotor voltages v_{qr} and v_{dr} independently. The rotor flux linkages and voltages can be expressed in terms of rotor currents as: $\psi_{dr} = \left(L_{rr} - \frac{L_m^2}{L_{ss}}\right) i_{dr} + \left(\frac{L_m}{L_{ss}}\right) \frac{V_s}{\omega_s}$ (19)

$$\psi_{dr} = \left(L_{rr} - \frac{L_m^2}{L_{ss}}\right) i_{qr}$$

$$v_{dr} = R_r i_{dr} + \left(L_{rr} - \frac{L_m^2}{L_{ss}}\right) \frac{di_{dr}}{dt} - s\omega_s \left(L_{rr} - \frac{L_m^2}{L_{ss}}\right) i_{qr} \tag{20}$$

$$v_{qr} = R_r i_{qr} + \left(L_{rr} - \frac{L_m^2}{L_{ss}}\right) \frac{di_{qr}}{dt} + s\omega_s \left(L_{rr} - \frac{L_m^2}{L_{ss}}\right) i_{dr} + s\left(\frac{L_m}{L_{ss}}\right) V_s$$

Where slip, $s = \frac{\omega_s - \omega_r}{\omega_s}$

Numerous control design schemes have been employed for variable speed Wind Energy Conversion Systems (WECS), primarily utilizing proportional integral (PI) controllers due to their established reliability and robust performance in the engineering domain. The optimization of parameter analysis has been conducted specifically on the rotor side converter PI controller to achieve optimal performance. It is assumed in this study that the grid-side converter controller effectively maintains the DC voltage at the reference level. Notably, the descriptions of the grid-side converter and pitch angle controller are not addressed in this analysis.

4.2. Power Control Scheme:

Variable speed operation of wind turbines offers the primary advantage of enhancing energy capture across a wide range of wind speeds. The power-speed characteristic serves as a dynamic reference for the generator power demand (reference value), which is determined based on the measured generator speed. It is now apparent from equation (17) that, with a constant stator flux linkage amplitude, the stator active power P_s can be controlled by adjusting the rotor axis current.

4.3. Terminal Voltage Control Scheme:

The terminal voltage controller is responsible for keeping the voltage at a reference level. Neglecting the stator resistance, the reactive power is provided in equation (18). The stator reactive power Q_s or terminal voltage V_s control is achieved by adjusting the rotor d-axis current(i_{dr}). This represents the principle of current control.

$$Q_s = -\left(\frac{L_m}{L_{ss}}\right) V_s i_{dr} + \left(\frac{1}{L_{ss}}\right)\frac{V_s^2}{\omega_s} \quad (21)$$

The reactive power generated by the wind turbine is directly dependent on i_{dr}:

$$Q_s = -\left(\frac{L_m}{L_{ss}}\right) V_s(i_{dr\_\mathrm{m}} + i_{dr\_\mathrm{g}}) + \left(\frac{1}{L_{ss}}\right)\frac{V_s^2}{\omega_s} \quad (22)$$

In equation (22), the direct component of the rotor current has been divided into two segments: one segment magnetizes the generator, while the other segment determines the net reactive power exchange with the grid. The magnitude of the direct component required to magnetize the generator itself is as follows: $i_{dr\_\mathrm{m}} = \frac{V_s}{\omega_s L_m}$.. (23)

The value of i_{dr_g}, which represents the reactive power generating portion of i_{dr}, dictates whether net reactive power is generated or consumed. Providing more or less reactive power to the grid will respectively raise or lower the terminal voltages.

4.4 Current Control Scheme:

The power and voltage controllers generate reference values for the q-axis and d-axis components of rotor current, respectively. These values are used in the current control scheme, which operates within the inner loop of the control system, as depicted in Figure 3. Within this scheme, the errors i_{qr} and i_{dr} are processed by the current regulators, resulting in the production of v_{qr} and v_{dr} by the controllers. To ensure accurate tracking of these currents, compensation terms are added to the controller outputs, yielding the reference value of the rotor voltages. This modified signal then adjusts the switching sequence to produce the necessary voltages at the converter's output. Therefore, precise estimation of current controller parameters is vital for optimizing system performance under conditions such as grid voltage sag, single-phase to ground faults, and changes in wind speed.

Control of Rotor Side Converter:

The primary objective of the rotor-side converter is to regulate the rotor current of the Doubly Fed Induction Generator (DFIG) for controlling both active and reactive power flow. This control is accomplished through inner fast current control loops oriented towards the d-axis stator flux. These inner loops regulate the rotor current components, while outer power control loops determine the reference rotor current components for the inner loops.

To formulate the rotor current control law, we eliminate i_s and ψ_r from equation (5) using equation (6) as described in reference (20) [21], resulting in the expression for V_r as follows:

$$V_r = R_r i_{r+}\sigma L_{rr}\frac{di_r}{dt} + \frac{L_m}{L_{ss}}\frac{d\psi_s}{dt} + js\omega_s\sigma L_{rr} i_r + js\omega_s\frac{L_m}{L_{ss}}\psi_s \quad (24)$$

Where, $$\sigma = \left(1 - \frac{L_m^2}{L_{ss}L_{rr}}\right) \quad (25)$$

Splitting voltage (24) into d – q component and neglecting derivative term at study state with

$\psi_{ds} = \psi_s \; and \; \psi_{qs} = 0$ lead to:

$$v_{dr}^* = R_r i_{dr}^* - s\omega_s\sigma L_{rr} i_{qr} \quad (26)$$

$$v_{qr}^* = R_r i_{dr}^* - s\omega_s\sigma L_{rr} i_{qr} + s\omega_s\left(\frac{L_m}{L_{ss}}\right)\psi_{ds} \quad (27)$$

In equations (26) and (27), v_{dr}^{*} and v_{qr}^{*} are the rotor voltage components in the reference frame necessary for achieving the desired reference rotor current values i_{dr_ref} and i_{qr_ref} in the rotor circuit. The terms involving $-s\omega_s\sigma L_{rr}\boldsymbol{i_{qr}}$ and $-s\omega_s\sigma L_{rr}\boldsymbol{i_{dr}}$ in equations (26) and (27) represent the cross coupling between the d and q components of the rotor voltage, respectively. The third term in equation (27) accounts for the speed-dependent induced electromotive force (emf.) associated with the stator flux. The cross coupling terms in equations (26) and (27) have smaller magnitudes compared to the back emf. term, exerting minimal influence on the control action executed by the Proportional-Integral (PI) controller in each axis. However, the third term in equation (27) acts as a disturbance to the output of the PI-controller in the q-axis, potentially leading to a steady-state tracking error even with high PI-controller gains [22]. To mitigate the impact of the back emf. term, it's feasible to introduce a feed-forward compensating term into the control law. This compensating term, as described in reference [21], is added to the output of the controller, effectively addressing the tracking error induced by variations in the back emf.

$$\text{feed forward term} = js\omega_s \frac{L_m}{L_{ss}}\boldsymbol{\psi_s} \tag{28}$$

Here, the controlled voltage equations can be represented as:

$$\boldsymbol{v_r} = \boldsymbol{v_r'} + js\omega_s\sigma L_{rr}\boldsymbol{i_r} + js\omega_s \frac{L_m}{L_{ss}}\boldsymbol{\psi_s} \tag{29}$$

The expression of reference voltages can be expressed as:

$$\boldsymbol{v_r} = K_{P\_RI}\boldsymbol{e} + K_{I\_RI}\int \boldsymbol{e}dt + js\omega_s\sigma L_{rr}\boldsymbol{i_r} + js\omega_s \frac{L_m}{L_{ss}}\boldsymbol{\psi_s} \tag{30}$$

The rotor current dynamics formed in the inner loop is represented by:

$$\sigma L_{rr}\frac{di_r}{dt} = \boldsymbol{v_r'} - R_r\, i_r \tag{31}$$

Here, the rotor current control loop approach using the Pl method is depicted in Figure 4. The dynamics of the inner loop shown in Figure 4 are represented by the function $G_{\_RI}(s)$.

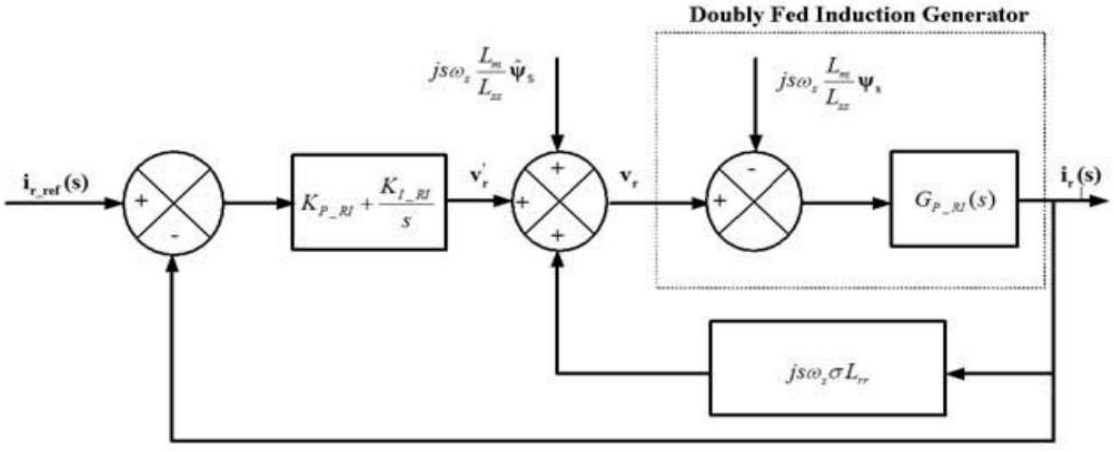

Fig. 4: Rotor side converter current control system

IV. OVERVIEW OF PARTICLE SWARM OPTIMIZATION:

Over the past two decades, several heuristic tools such as evolutionary computation, simulated annealing, tabu search, and particle swarm optimization (PSO) have evolved, enabling the solution of optimization problems that were previously challenging or impossible to solve. The application of these tools offers two major advantages: the ability to develop solutions much faster than traditional approaches and robustness, as they are relatively insensitive to noisy or missing data. PSO, in particular, is a heuristic search method inspired by the swarming behavior of

biological populations. It was developed through the simulation of a simplified social system and has been found to be robust in solving continuous nonlinear optimization problems. PSO, proposed by Kennedy and Eberhart in the mid-1990s, is based on the objective function and has proven to be highly effective in solving a wide range of engineering problems. The method was initially conceived while studying the choreographed, graceful motion of bird swarms as part of a socio-cognitive investigation into the concept of "collective intelligence" in biological populations [8-9].

The Particle Swarm Optimization (PSO) algorithm optimizes an objective function through a population-based search method, moving from one set of points to another in a single iteration with potential improvements using deterministic and probabilistic rules. The population, known as a swarm, consists of potential solutions represented by particles, which metaphorically mimic birds in flocks. Initially, the PSO algorithm randomly initializes a population of particles, allowing them to freely navigate through the multidimensional search space. During their flight, each particle updates its velocity and position based on its own best experience and that of its peers, aiming to converge towards the region with the best objective function value. PSO relies on basic mathematical operators and is computationally efficient in terms of both memory usage and speed. It typically yields high-quality solutions in shorter calculation times and demonstrates stable convergence characteristics compared to other stochastic methods [9, 23].

4.1. Initialization:

During the initialization process, the swarm particles are randomly distributed within predefined ranges across the design space, as described in equations (32) and (33).

$$x_0^i = x_{min} + rand(x_{max} - x_{min}) \tag{32}$$

$$v_0^i = \frac{[x_{min} + rand(x_{max} - x_{min})]}{\Delta t} = \frac{Position}{Time} \tag{33}$$

Where, $x_k^i \ and \ v_k^i \ \rightarrow$ randomly generated positions and velocities of the initial swarm's particles.

$x_{min} \ and \ x_{max} \ \rightarrow$ upper and lower bounds on the design variables values.

rand $\rightarrow$ random parameters, a uniformly distributed random variable between 0 and 1.

In a vector format superscript and subscript denoting the i^{th} particle at time k respectively.

4.2. Velocity updating:

The velocity of all particles at time k+1 is updated using the particle's objective function value, which depends on the particle's current position in the design space at time k .

Each particle maintains a record of its coordinates in the design space, associated with the best solution obtained so far during its trajectory, including the current and all previous moves. This best position of the particle achieved thus far is referred to as the local best value P_{best}^i. Additionally, a global best value, denoted as P_{best}^g, and its corresponding location, represent the best solution obtained by any particle in the current swarm. The velocity update formula for each particle in the swarm incorporates these two pieces of information—particle memory influence and swarm influence—along with the effect of current motion v_k^i to provide a search direction v_{k+1}^i for the next iteration, as depicted in equation (34).

Velocity of particle

$$\text{i at time k+1} \ \rightarrow \ v_{k+1}^i = \underbrace{wv_k^i}_{\text{current motion}} + \underbrace{c_1 rand \frac{\left(p^i - x_k^i\right)}{\Delta t}}_{\text{particle memory influence}} + \underbrace{c_2 rand \frac{\left(p_k^g - x_k^i\right)}{\Delta t}}_{\text{swarm influence}} \tag{34}$$

Where, $p_k^g \ \rightarrow$ best global value in the current swarm

p^i → best position of i^{th} particle over time, i.e in current and all previous moves.

rand → random parameter, a uniformly distributed random variable between 0 and 1. Wande, w, c_1 *and* c_2 → three weight factors, namely, inertia factor, self confidence factor and swarm confidence factor, respectively.

The values of w, c_1 *and* c_2 suggests upper and lower bounds and the proper setting these three weight factors provides the best convergence rate for the problem considered.

Other combinations of values typically result in significantly slower convergence or, in some cases, non-convergence altogether. The parameters c_1 *and* c_2 determine the relative influence of the local best P_{best}^i and the global best P_{best}^g, while the inclusion of parameters r_1 and r_2 allows the PSO to stochastically vary these influences.

5.3. Position Updating:

The position of each particle is updated using its velocity vector, as described in equation (35) and illustrated in Figure 6:

$$x_{k+1}^i = x_k^i + v_{k+1}^i \Delta t \quad (35)$$

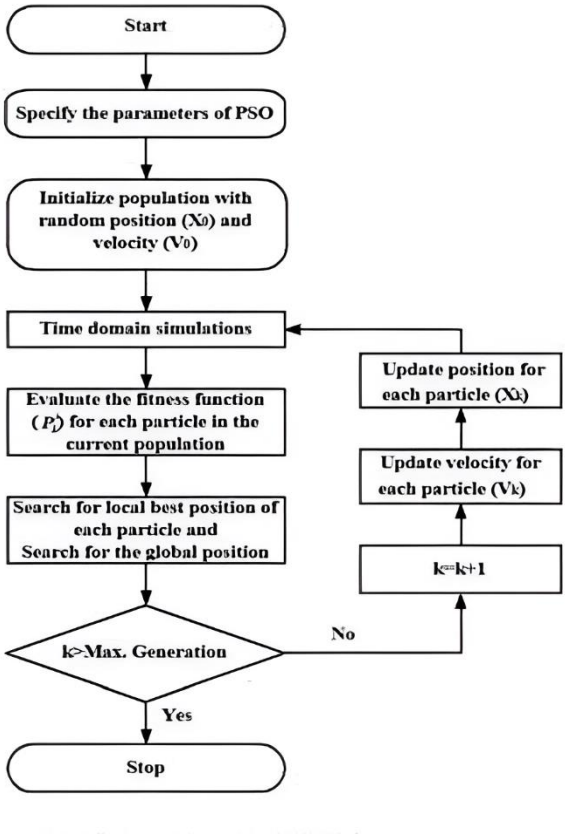

Fig.5: Flow chart of PSO

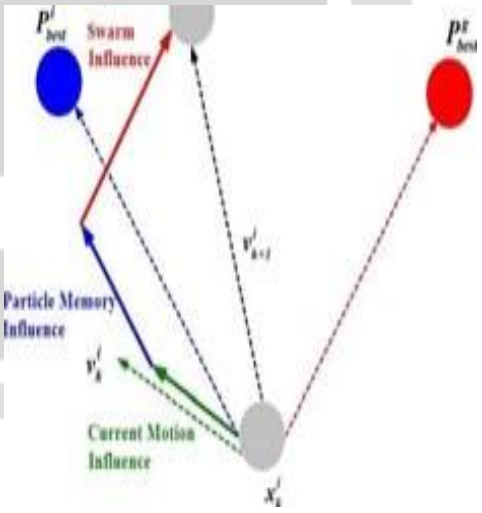

Fig.6: Depiction of the velocity and position updates in PSO

5.4. Memory Updating:

Each particle has a memory and is capable of remembering the best position in the search space it has ever visited. The local best position, p_{best}^i and the global best position p_{best}^g are updated as shown in equations (36) and (37), respectively:

$$p_{best}^i = p_k^i \quad if\ f(p_k^i) < f(p_{best}^i) \quad (36)$$

$$p_{best}^g = p_k^g \quad if\ f(p_k^g) < f(p_{best}^g) \quad (37)$$

Where, $f(x)$ is the objective function subject to minimization.

5.5 Termination Checking:

The three steps of velocity update, position update, and fitness calculations for memory updating are repeated until a desired convergence criterion is achieved. Once the algorithm terminates, it reports the values of the global best position p_{best}^{g} and the fitness function value $f(p_{best}^{g})$ as its solution.

VII. RESULT:

The Particle Swarm Optimization (PSO) method is employed to optimize the parameters of the rotor-side converter current controller, aiming to enhance system performance, as outlined in equations (38) and (39), along with the associated constraints. The performance of the system is evaluated using step input performance measures, including transient and steady-state dynamics, peak overshoot ratio, rise time, peak time, settling time, and steady-state error, for the two objective functions specified in Table 2.

Table 2: Performance measures for controller performance

Method	Rise Time (ms)	Peak Time (ms)	Settling Time (ms)	Peak Overshoot	Steady State Error
Pl Controller	6.52	14.79	65.38	0.0972	5.08e-07
PSO tuned Pl with Objective Function I	5.58	14.21	64.54	0.0997	4.64e-07
PSO tuned Pl with Objective Function2	5.59	14.16	64.78	0.0924	3.88e-07

It is clear from the analysis of performance measures that PSO tuned PI controller, with both the objective functions, is giving better results than Pl controller. The optimized controller parameters, obtained using objective functions in (18) and (39), are given in Appendix. The best results are considered here for WECS equipped with DFIG during optimization process.

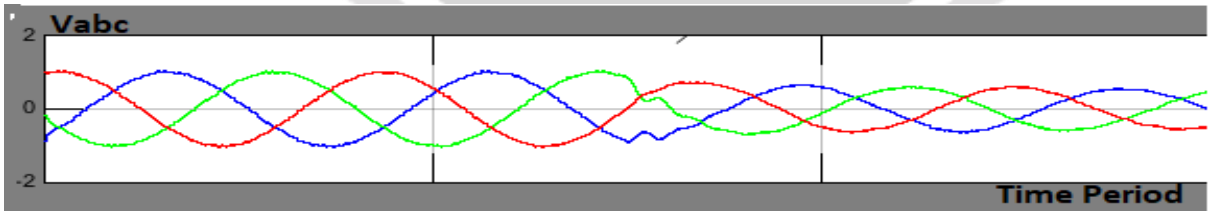

Fig.7: Stator Voltage

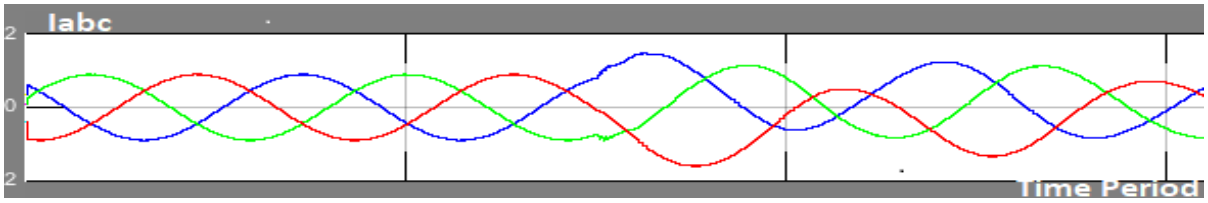

Fig.8: Stator Current

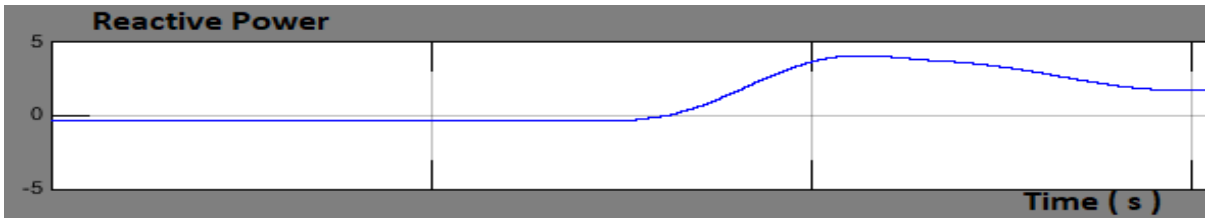

Fig.9: Reactive Power

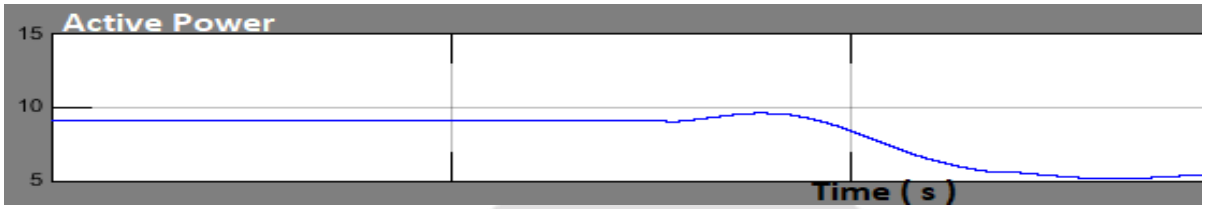

Fig.10: Active Power

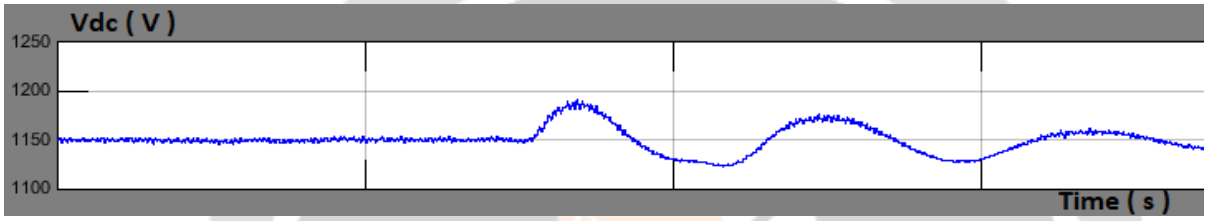

Fig.11: DC Voltage

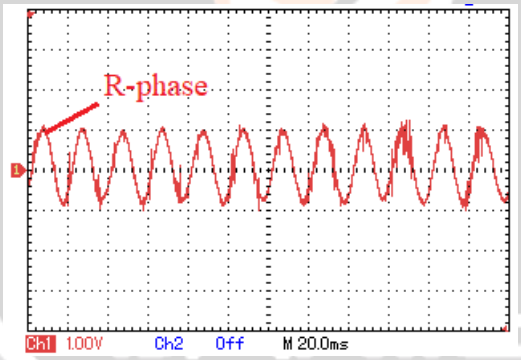

Fig.12: DFIG Stator Current (Experimental Waveform)

The dynamic response analysis depicted in Figure 8 reveals that the response during a grid voltage sag caused by a remote fault is significantly enhanced, with faster response times and reduced settling times observed with the PSO-tuned PI controller parameters. A similar improvement in performance is evident in the case of a single-phase-to-ground fault, as shown in Figure 9. The power tracking behavior due to wind speed changes in both cases is nearly identical, as illustrated in Figure 10. The optimally controlled system exhibits good damping and dynamic characteristics within the system's limitations.

VI. CONCLUSION:

This paper provides a comprehensive description of the dynamic model and control system structure for a variable speed Wind Energy Conversion System (WECS) equipped with a Doubly Fed Induction Generator (DFIG). The rotor-side decoupled power control equations are derived in the stator flux orientation system. Using these equations and transfer functions, the rotor-side decoupled control system is developed using conventional design procedures. Particle Swarm Optimization (PSO) is employed to tune the parameters of the rotor-side converter PI current controller. To achieve this, an optimization problem is formulated using suitable objective functions and constraints. The system is then simulated under various test conditions, including grid voltage sag resulting from a remote fault,

single-phase-to-ground fault, and wind speed changes, using both the PI controller and the PSO-optimized PI controllers. The studies conducted under these conditions highlight the importance of tuning the controller parameters, with the improvements reflected in the form of better performance measures of the system response.

VII. ACKNOWLEDGEMENTS

The authors recognize the monetary help from the Power Plant Engineering works, Visakhapatnam, Andhra Pradesh, India" through research project no: 11/2019-20.

VIII. REFERENCES:

1. World Wind Energy Association, 2016, http://www.wwindea .org/wwea-half-year-report-worldwind-wind-capacity-reached456-gw.
2. T. Ackerman, Wind Power in Power Systems, John Wiley and Sons Ltd, England, UK, 2005.
3. K. E. Okedu and U. Roland, “Low voltage ride through methods for DFIG VSWT,” Journal of Emerging Trends in Engineering and Applied Sciences, vol. 5, no. 8, pp. 221–226, 2014.
4. D. A. Rivkin, L. D. Anderson, and L. Silk, Wind Turbine Control Systems, Jones and Bartlett Learning, Massachusetts, Mass, USA, 2013.
5. Vestas Wind Systems A/S, 2014, https://www.vestas.com/ en/products/turbines.
6. Bonanomi, “Powerful analysis of wind turbine gearboxes,” Power TransmissionWorld, 2014, http://www.powertransmissionworld.com/powerful-analysis-of-wind-turbine-gearboxes/
7. F. Blaabjerg, M. Liserre, and K. Ma, “Power electronics converters for wind turbine systems,” IEEE Transactions on Industry Applications, vol. 48, no. 2, pp. 708–719, 2012.
8. J. Zhang, G. Chen, and X. Cai, “Thermal smooth control for Multi-MW parallel wind power converter,” in Proceedings of the 2013 IEEE International Conference of IEEE Region 10, IEEE TENCON 2013, pp. 1–4, October 2013.
9. T. Lei, M. Barnes, and A. C. Smith, “Thermal cycling evaluation for DFIG wind turbine power converter based on joint modelling,” in Proceedings of the 5th Annual IEEE Energy Conversion Congress and 3, ECCE 2013, pp. 3845–3851, usa, September 2013.
10. Y. M. Alsmadi, L. Xu, F. Blaabjerg, A. P. Ortega, and A. Wang, “Comprehensive analysis of the dynamic behavior of gridconnected DFIG-based wind turbines under LVRT conditions,” in Proceedings of the 7th Annual IEEE Energy Conversion Congress and Exposition, ECCE 2015, pp. 4178–4187, can, September 2015.
11. S. Sharma, J. P. Mishra, and S. Datta, “Sliding mode power control of a DFIG based variable speed wind energy conversion system,” in Proceedings of the 12th IEEE International Conference Electronics, Energy, Environment, Communication, Computer, Control, INDICON ’15, December 2015. A. Gupta, S. N. Singh, and D. K. Khatod, “Modeling and simulation of doubly fed induction generator coupled with wind turbine-An overview,” Journal of Engineering, Computers & Applied Sciences, vol. 2, no. 8, 2013.
12. K. E. Okedu, “Applications of wind power generation in grid connected power system,” The Pacific Journal of Science and Technology, vol. 13, no. 2, 2012.
13. T. Burton, N. Jenkins, D. Sharpe, and E. Bossanyi, Wind Energy Handbook, John Wiley and Sons Ltd, England, UK, 2nd edition, 2011.
14. Petersson, Analysis, modeling and control of doubly-fed induction generators for wind turbines [Ph.D. thesis], Chalmers University of Technology, Goteborg, Sweden, 2005. ¨
15. K. E. Okedu, R. Takahashi, J. Tamura, and S. M. Muyeen, “Comparative study on current and voltage controlled voltage source converter based variable speed wind generator,” in Proceedings of the 2011 2nd International Conference on Electric Power and Energy Conversion Systems, EPECS ’11, November 2011.
16. J. J. Justo, F. Mwasilu, and J.-W. Jung, “Doubly-fed induction generator based wind turbines: a comprehensive review of fault ride-through strategies,” Renewable and Sustainable Energy Reviews, vol. 45, pp. 447–467.